Bull. Mater. Sci. (2022) 45:172
https://doi.org/10.1007/s12034-022-02741-1

Turning of luminescence properties of $Ba_2V_2O_7$ phosphors by co-doping Eu^{3+}/Dy^{3+} ions

N VENKATESH BHARATHI[1,3], P KAVITHA[2], S RAMASWAMY[1,3], S S JAYABALAKRISHNAN[2] and K SAKTHIPANDI[4,*]

[1]P G and Research Department of Physics, N M S S V N College, Madurai 625 019, India
[2]Department of Physics, M T N College, Madurai 625 004, India
[3]Post Graduate Department of Physics, M T N College, Madurai 625 004, India
[4]Department of Physics, SRM TRP Engineering College, Tiruchirappalli 621 105, India
*Author for correspondence (sakthipandi@gmail.com)

MS received 31 January 2022; accepted 1 May 2022

Abstract. A series of $Ba_{1.97-x}Eu_{0.03}Dy_xV_2O_7$ (x = 0.01, 0.02, 0.03, 0.04 and 0.05) phosphor materials were synthesized by hydrothermal method. Phase purity, structural, optical and luminescence characteristics of as-synthesized phosphors have been studied using powder X-ray diffraction (PXRD), UV–visible spectroscopy and fluorescence spectrometry. The XRD patterns of as-synthesized phosphors were indexed and predicted as triclinic structure. The broad absorption in the UV region was originated from $[VO_4]^{3-}$ group charge transfer and the sharp peaks observed in the visible to near-infrared (NIR) region was originated from Eu^{3+}/Dy^{3+} ions charge transfer. In photoluminescence (PL) spectra, the broad emission peak observed from 400 to 570 nm was due to the charge transfer band of $[VO_4]^{3-}$ group. A sharp peak observed from 570 to 710 nm were due to the charge transition of Eu^{3+}/Dy^{3+} ions. The PL spectra recorded for different excitations at 268, 344, 335, 346, 346 and 339 nm, emitted bluish white colour with slight changes in its Commission International de l′Eclairage coordinate values. The white colour emission of $Ba_{1.97-x}Eu_{0.03}Dy_xV_2O_7$ phosphors was observed by the irradiation under the UV light 365 nm. Hence, the results have suggested that the as-prepared phosphor materials are the potential candidates in the fabrication of a UV or near-UV chip-excited white light-emitting diode.

Keywords. Hydrothermal method; luminescence; charge transfer transition; WLEDs.

1. Introduction

White-light emitting diode (WLED) has been considered as a next generation of lighting source in recent years due to considerable merits like high energy saving, easy maintenance, long durability, efficient conversion of electrical energy to light, eco-friendly, less electrical consumption [1–3]. In general, the commercially available WLEDs can be obtained by GaN blue LED and $Y_3Al_5O_{12}:Ce^{3+}$ yellow phosphors combination [4–6]. In this type of WLEDs, due to red emission deficiency it exhibits poor colour rending index (CRI) of less than 80% and high correlated colour temperature (CCT) of above certain temperature [7,8]. To fulfill these issues, many researchers were constantly working to prepare a novel red, green and blue (RGB) emission in a single-component material and it may be the direction of solid-state lighting development.

So far, considerable interest in inorganic materials doped with trivalent lanthanide shows an excellent luminescent properties. Basically, lanthanide ion exhibits the transitions within the partially filled $4f^n$ inner shell. These parity forbidden transitions were attributed the low molar absorption coefficient and efficient luminescent lifetime [9–11]. Various attempts show that Eu^{3+} ion exhibits an intense red emission in the visible region due to $^5D_0 \rightarrow {}^7F_J$ (J = 0, 1, 2, 3, 4) transitions [12,13]. Similarly, Dy^{3+} ion also exhibits three emission colours in the visible region of blue $^4F_{9/2} \rightarrow {}^6H_{15/2}$, yellow $^4F_{9/2} \rightarrow {}^6H_{13/2}$ and red $^4F_{9/2} \rightarrow {}^6H_{11/2}$ emissions [14,15].

Many studies on Eu^{3+}/Dy^{3+} co-doped phosphors with diverse host materials have been published to date. Chang Chengkang *et al* [16] studied the photoluminescence (PL) properties of Eu^{3+}/Dy^{3+} co-doped $Sr_3Al_2O_6$ phosphor and synthesized it. Meza-Rocha *et al* [17] created/fabricated a multicolour luminescence of potassium-zinc phosphate glasses activated with Eu^{3+}, Dy^{3+} and Dy^{3+}/Eu^{3+}. Nannan Yao and colleagues [18] produced ZnO: Eu^{3+}, Dy^{3+} material for solar cell applications and improved efficiency of the of dye-sensitized solar cells, about 212 and 245% higher than pure TiO_2 and about 91.4 and 105% higher than with TiO_2/graphene (G) structure, respectively.

Sun Xin-Yuan *et al* [19] used a solid-state process to successfully synthesize Dy^{3+}, Eu^{3+}- doped, and Eu^{3+}/Dy^{3+}-co-doped $SrGd_2O_4$ scintillating phosphors and

Published online: 02 September 2022

investigated its luminescence properties. Zhai Yongqing *et al* [20] studied the luminous characteristics of $ZnWO_4$:-Eu^{3+}, Dy^{3+} materials, which they synthesized using a hydrothermal technique for WLED applications. The PL properties of Eu^{3+}, Dy^{3+}-activated $Ca_3La(VO_4)_3$ phosphors for WLED were produced and examined by Vengala Rao *et al* [21]. Wang Huayu *et al* [22] have investigated PL properties, energy transfer and synthesized Eu^{3+}/Dy^{3+}-co-doped $NaGd(MoO_4)_2$ phosphors for solid-state lighting application [22]. The above all, it is inferred that the desired wavelength of the light is attained by adjusting/modifing the ratio of Dy^{3+} ions co-doping concentration with Eu^{3+} ions [14,15].

Inorganic luminescent materials, such as alkaline earth metal vanadates containing Ln^{3+} ions, have recently become a popular choice for WLED applications. These materials have a significant potential for usage as a single-component WLED material because of their excellent luminescence [23–25]. Among various alkaline earth metal vanadates, $M_2V_2O_7$ (M = Ca, Sr, Ba) phosphors were widely used in filter, antenna, solid-state lighting [26–28] and other applications. In the previous work, the self-activated $Ba_2V_2O_7$ phosphor was found to be an effective and excellent luminescent material for ultra-violet (UV)-chip-excited WLED. This phosphor has a broad absorbance in the UV region and a broad emission in the visible region [29]. The drawback found in $Ba_2V_2O_7$ phosphor material was the insufficient red emission in the visible spectrum. To overcome this problem, an attempt was made to synthesize $Ba_{2-x}Eu_{0.03}Dy_xV_2O_7$ (BEDVO) phosphor doped with the fixed concentration of europium (Eu^{3+}) ion (x = 0.03) and varied the concentration of dysprosium (Dy^{3+}) ion as a co-doped. In this present investigation, $Ba_{2-x}Eu_{0.03}Dy_xV_2O_7$ (x = 0.01, 0.02, 0.03, 0.04 and 0.05) phosphor was synthesized by hydrothermal method. The structural, optical and photoluminescent properties were investigated for WLED applications.

2. Experimental

2.1 *Materials*

Barium nitrate ($Ba(NO_3)_2$), sodium metavanadate ($NaVO_3$), europium oxide (Eu_2O_3), dysprosium oxide (Dy_2O_3) and ammonia solution (NH_4) purchased from LOBA chemicals (analytical grade), India, with high purity (99%) were used without any further purification. Distilled water was used as the solvent throughout the synthesis protocol.

2.2 *Preparation of BEDVO phosphor*

$Ba_{2-x}Eu_{0.03}Dy_xV_2O_7$ (x = 0.01, 0.02, 0.03, 0.04 and 0.05) phosphor was prepared by using the hydrothermal method. $Ba(NO_3)_2$ (8.19 g) and $NaVO_3$ (1.95 g) were dissolved in 40-ml distilled water separately and the mixed solutions were stirred for 15 min. Eu_2O_3 (0.085 g) was dissolved in 2 ml of nitric acid and they were mildly heated to obtain europium nitrate. Similarly, 0.029 g of Dy_2O_3 was dissolved in 2 ml of nitric acid and they were mildly heated to obtain dysprosium nitrate. These dysprosium nitrate and europium nitrate mixtures were then added to the mixed source materials under vigorous stirring. The pH level was adjusted to about 12 by using the ammonia solution with continuous stirring. After adjusting pH, the solution was stirred for 1 h. The mixed solution was transferred into 100 ml Teflon-lined autoclave and it was tightly sealed. The solution in the autoclave was heated at 180°C for 48 h in a muffle furnace, which was then cooled to room temperature naturally. The precipitate was filtered and washed several times with distilled water. The final white colour powder was obtained after drying at 60°C on a hot plate for few hours.

2.3 *Characterization techniques*

PANalytical Xpert-Pro diffractometer with Cu-K radiation in the scan range of 10°–60° is used to analyse X-ray diffraction (XRD) investigations for the BEDVO phosphors. The diffused reflectance spectra were recorded from 200 to 1200 nm range using a UV-2600 SHIMADZU spectrophotometer with an aid of $BaSO_4$ as a non-absorbing standard reference. A Shimadzu RF-5301PC spectrofluorometer is used to record PL spectra. The chromaticity colour coordinates of the Commission International de l'Eclairage (CIE) were determined using the GOCIE Version 2 CIE-1931 plot programme. At room temperature, all measurements were taken.

3. Results and discussion

3.1 *Structural analysis*

Powder X-ray diffraction (PXRD) is a versatile, non-destructive analytical method for identification and quantitative determination of various crystalline forms in the phosphors. Figure 1a shows the PXRD patterns of the as-synthesized phosphors. All the PXRD profiles were well indexed to triclinic crystal structure [JCPDS card no.: 76-0612] of the parent element $Ba_2V_2O_7$ phosphor. The additional peaks or traces corresponding to Eu^{3+} and Dy^{3+} ions are absent in figure 1a. Further, it was clearly evident that, as concentration of Dy^{3+} dopant increases, the diffraction peaks were slightly shifted towards the lower angle side, as shown in figure 1b. This peak shifting and line broadening were due to the partial replacement of the higher ionic radii (Ba^{2+}; r = 0.14 nm) ions by lower ionic radii (Eu^{3+}; r = 0.095 nm and Dy^{3+}; r = 0.108 nm) ions [30,31]. This observation obeys the Vegard's law [32]. Similar observations were reported by Taniguchi Kouta *et al* [33],

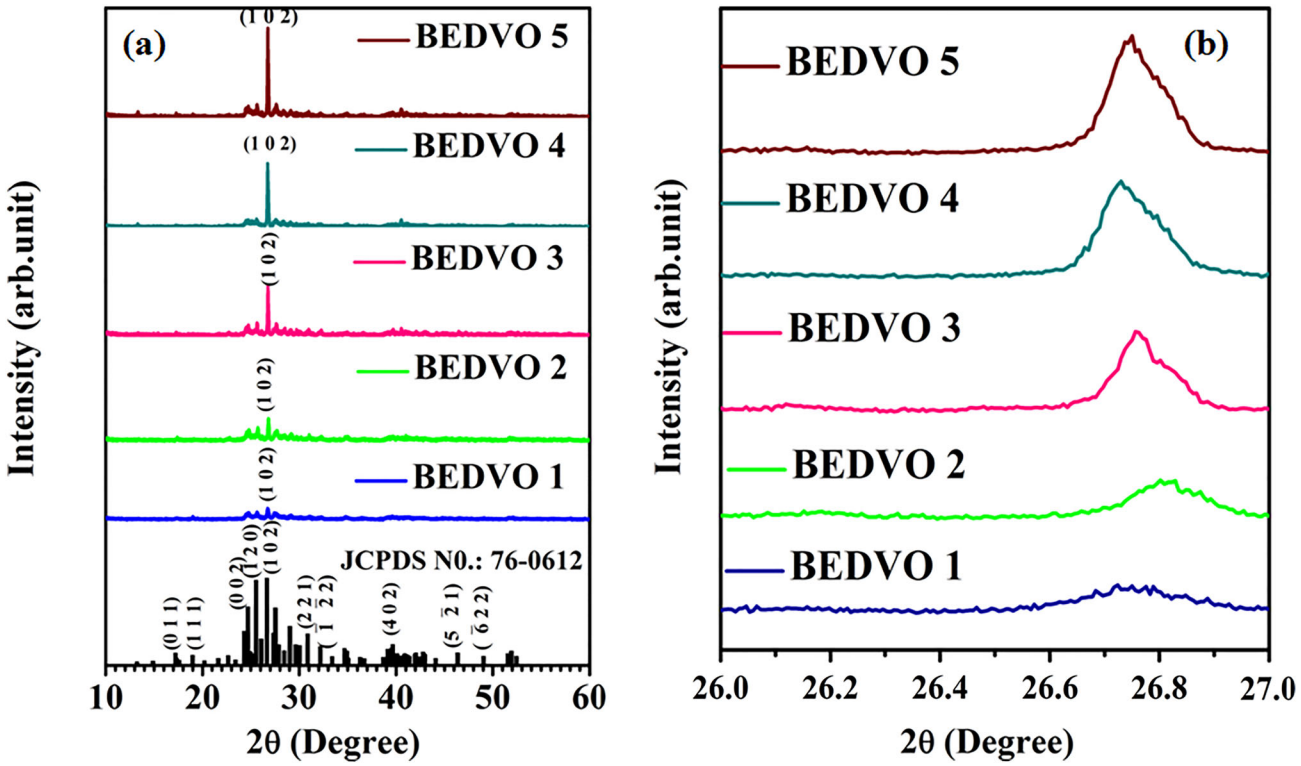

Figure 1. (**a**) Powder XRD patterns of BEDVO phosphors. (**b**) The enlarged view of peaks in the 2θ range (26–27°).

Kazuki Sakoda and Masanori Hirano [34] and Fang Mu-Huai *et al* [35] for the samples $Sr_{1-x}Eu_xGa_2S_4$, $Zn(Al_xGa_{1-x})_2O_4$ and $SrLi(Al_{1-x}Ga_x)_3N_4$:Eu^{2+}, respectively. Further, it can be marked from the increase in relative intensity of (102) XRD peak that the increase in Dy^{3+} doping concentration leads to an increase in the crystalline nature of the samples.

The acceptable percentage difference (D_r) between radii of Eu^{3+}/Dy^{3+} dopant ion and Ba^{2+} substituted ion should not be more than 30%, which was obtained by equation (1):

$$D_r = \frac{R_s - R_d}{R_s} \times 100\%, \tag{1}$$

where R_s is the radius of substituted ion and R_d is the radius of dopant ion [36]. The estimated value of D_r for Eu^{3+}/Dy^{3+} dopant phosphor was found to be 28 and 22%, respectively. Thus, it was confirmed that the Eu^{3+}/Dy^{3+} ions have been successfully incorporated into the Ba^{2+} lattice site in the $Ba_2V_2O_7$ host without any structural change.

3.2 *UV–visible-NIR spectral analysis*

Figure 2a shows the diffused reflectance spectra of the as-synthesized BEDVO phosphors from UV to NIR region, i.e., 200–1200 nm. The absorption peak centred at 215 nm was due to the fraction of electronic charge transferred between donor and acceptor (CT) in $O^{2-} \rightarrow Eu^{3+}/Dy^{3+}$ ions [37]. The broadband observed in the range of 241 to 350 nm centred at 296 nm was due to the CT between $^1A_1 \rightarrow {}^1T_1$ and $^1A_1 \rightarrow {}^1T_2$ in the VO_4 tetrahedral group [38,39]. Further, small peaks were also observed in the visible to NIR region, i.e., 400–1200 nm [40]. The enlarged view of this region is shown in figure 2b. The appearance of the peaks at 469, 537 and 574 nm was attributed to $^7F_0 \rightarrow {}^5D_2$, $^7F_1 \rightarrow {}^5D_1$ and $^7F_0 \rightarrow {}^5D_0$ transitions of Eu^{3+} ion, respectively. Also, the peaks appeared at 802, 909 and 1108 nm were corresponding to $^6H_{15/2} \rightarrow {}^6F_{5/2}$, $^6H_{15/2} \rightarrow {}^6F_{7/2}$ and $^6H_{15/2} \rightarrow {}^6F_{7/2,\ 9/2}$ transitions of Dy^{3+} ion, respectively [41–43]. It was confirmed that the formation of the meta-stable state between the valence band and the conduction band is due to the substitution of Eu^{3+}/Dy^{3+} ions.

Further, the absorption coefficient of BEDVO phosphors can be achieved using Kubelka–Munk function, expressed as in equation (2):

$$F(R) = \frac{K}{S} = \frac{(1-R)^2}{2R}, \tag{2}$$

where K, S and R represent the absorption coefficient, scattering coefficient and observed reflectivity, respectively [37,44].

The absorption coefficient ($F(R)$) and the optical bandgap (E_g) of the as-prepared BEDVO phosphors can be related by Tauc relation, expressed as in equation (3):

$$(h\upsilon F(R))^{1/n} = A(h\upsilon - E_g), \tag{3}$$

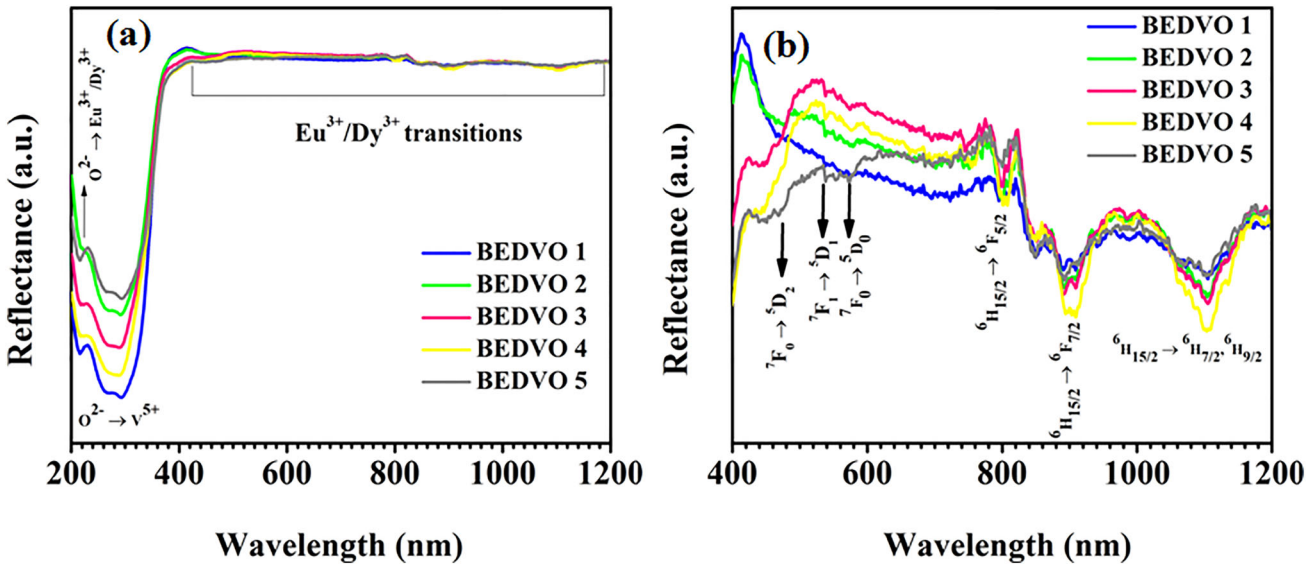

Figure 2. (**a**) The diffuse reflectance spectra and (**b**) the enlarged view of peaks in the range 400–1200 nm of BEDVO phosphors.

where $F(R)$ is the absorption coefficient, A the proportionality constant, $h\upsilon$ is the photon energy, E_g the bandgap energy. The value of n is ½ for direct-type transition and 2 for an indirect-type transition. The estimated bandgap values of the as-synthesized phosphors are shown in figure 3. The estimated values of the bandgap energy BEDVO phosphors were 3.57, 3.42, 3.38, 3.32 and 3.27 eV, respectively, for x = 0.01, 0.02, 0.03, 0.04 and 0.05. There were two significant reasons for the decrease in the bandgap (indirect bandgap) values; one is the formation of metastable state between the valence band and the conduction band (i.e., in between direct bandgap) and the other is the formation of the distorted VO_4 tetrahedral group due to the influence of the dopant ion [45,46].

3.3 *PL spectral analysis*

Figure 4 shows the excitation spectra of the as-prepared BEDVO phosphors monitored under 574 nm excitation wavelength. All the excitation spectra consist of the intense broad band peak in the range of 300 to 390 nm, which was due to the CT of $O^{2-} \rightarrow V^{5+}$ bond in the host matrix. When the concentration of Dy^{3+} increased, the sharp peak at 286 nm for x = 0.02 concentration reachs maximum, which was due to the second-harmonic generation [47–49]. This indicates that these phosphors could be excited by the near-UV light along with the charge transfer band, which might find application in solid-state lighting.

The emission spectra of the as-synthesized BEDVO phosphors were recorded with UV excitation wavelength at

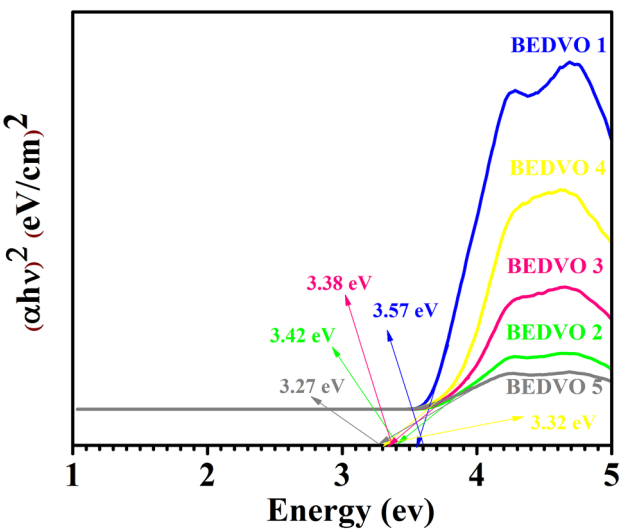

Figure 3. The Tauc plot for determining the bandgap of BEDVO phosphors.

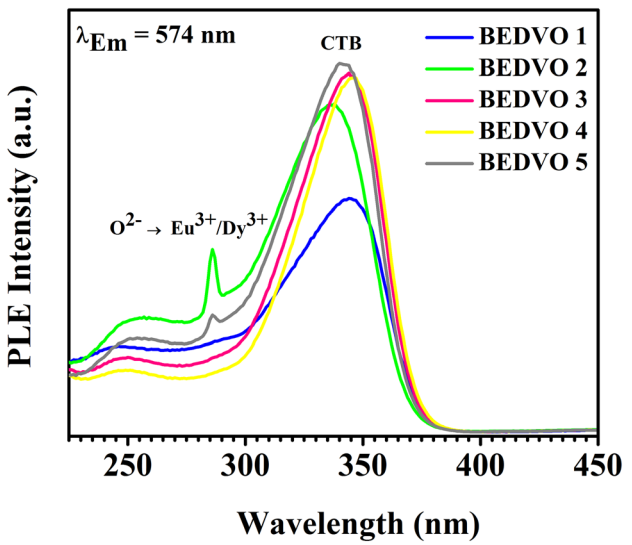

Figure 4. PLE spectra of BEDVO phosphors monitored at 574 nm emission.

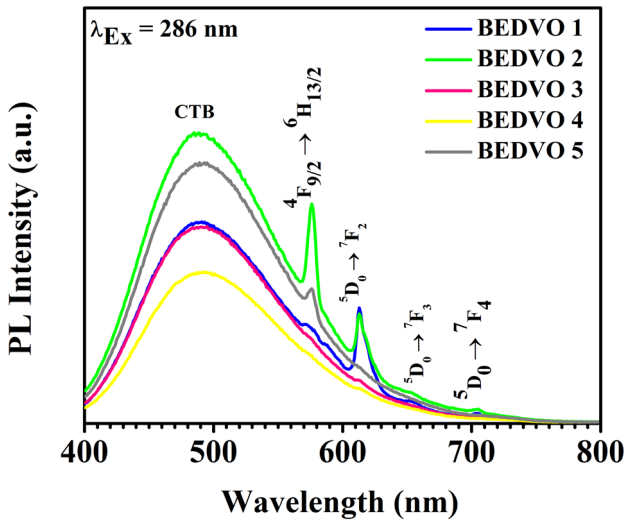

Figure 5. The PL spectra of BEDVO phosphors monitored at 286 nm.

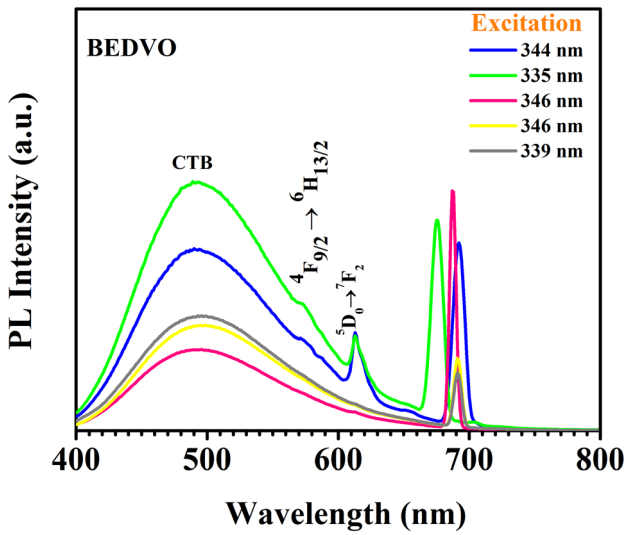

Figure 6. The PL spectra of BEDVO phosphors monitored at 344, 335, 346, 346 and 339 nm excitations.

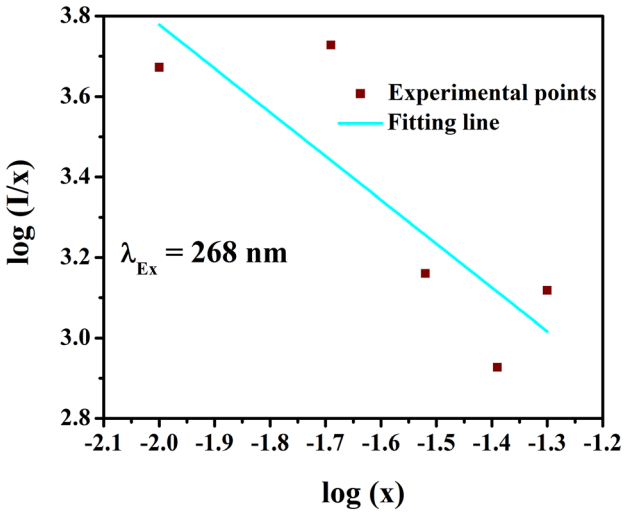

Figure 7. Dependence of log(*I*/*x*) on log(*x*) of BEDVO phosphors under 268 nm excitation.

286 nm, depicted in figure 5. The intense broad band peak was obtained in the range of 400 to 568 nm for all the phosphors. Figure 6 shows the emission spectra of the as-prepared BEDVO phosphors excited at 344, 335, 346, 346 and 339 nm, respectively. Here, the broad and few intense peaks were obtained in the emission spectra. The broad peak centred at 493 nm was due to the localized energy transfer between V^{5+} and O^{2-} in the VO_4 tetrahedral group. The observed peaks in figures 4 and 5 are listed in table 1, along with its CT and bandgap measured [50–57].

Figure 6 shows that when the Eu^{3+} doping concentration increased, the broad emission peak intensity rised to a maximum of $x = 0.02$ concentration, after which the peak intensity declined. The peak intensity of the dopant transition peaks was found to increase maximum up to $x = 0.02$ concentration, however as the doping concentration was increased further, the peak intensity was found to decrease due to the concentration quenching effect. Similarly, the transition $^5D_0 \rightarrow {}^7F_4$ was pushed into the high energy

Table 1. Emission spectra of the as-synthesized BEDVO phosphors [50–57].

Excitation wavelength (nm)	Emission peaks in wavelength	Charge transition	References
286	The broad band peak (400–568 nm)	$^3T_2 \rightarrow {}^1A_1$ and $^3T_1 \rightarrow {}^1A_1$ due to VO_4 group	[50]
	574 nm	$^4F_{9/2} \rightarrow {}^6H_{13/2}$ due to Dy^{3+} ion	[51,52]
	613 nm	$^5D_0 \rightarrow {}^7F_2$ due to Eu^{3+} ion	[52,53]
	656 nm	$^5D_0 \rightarrow {}^7F_3$ due to Eu^{3+} ion	[54–56]
	703 nm	Due to the second-harmonic generation	[57]
344, 335, 346 and 339	The broad band peak (400–568 nm)	$^3T_2 \rightarrow {}^1A_1$ and $^3T_1 \rightarrow {}^1A_1$ due to VO_4 group	[50]
	574 nm	$^4F_{9/2} \rightarrow {}^6H_{13/2}$ due to Dy^{3+} ion	[51,52]
	613 nm	$^5D_0 \rightarrow {}^7F_2$ due to Eu^{3+} ion	[52,53]
	676 nm	$^5D_0 \rightarrow {}^7F_4$ due to Eu^{3+} ion	[54–56]

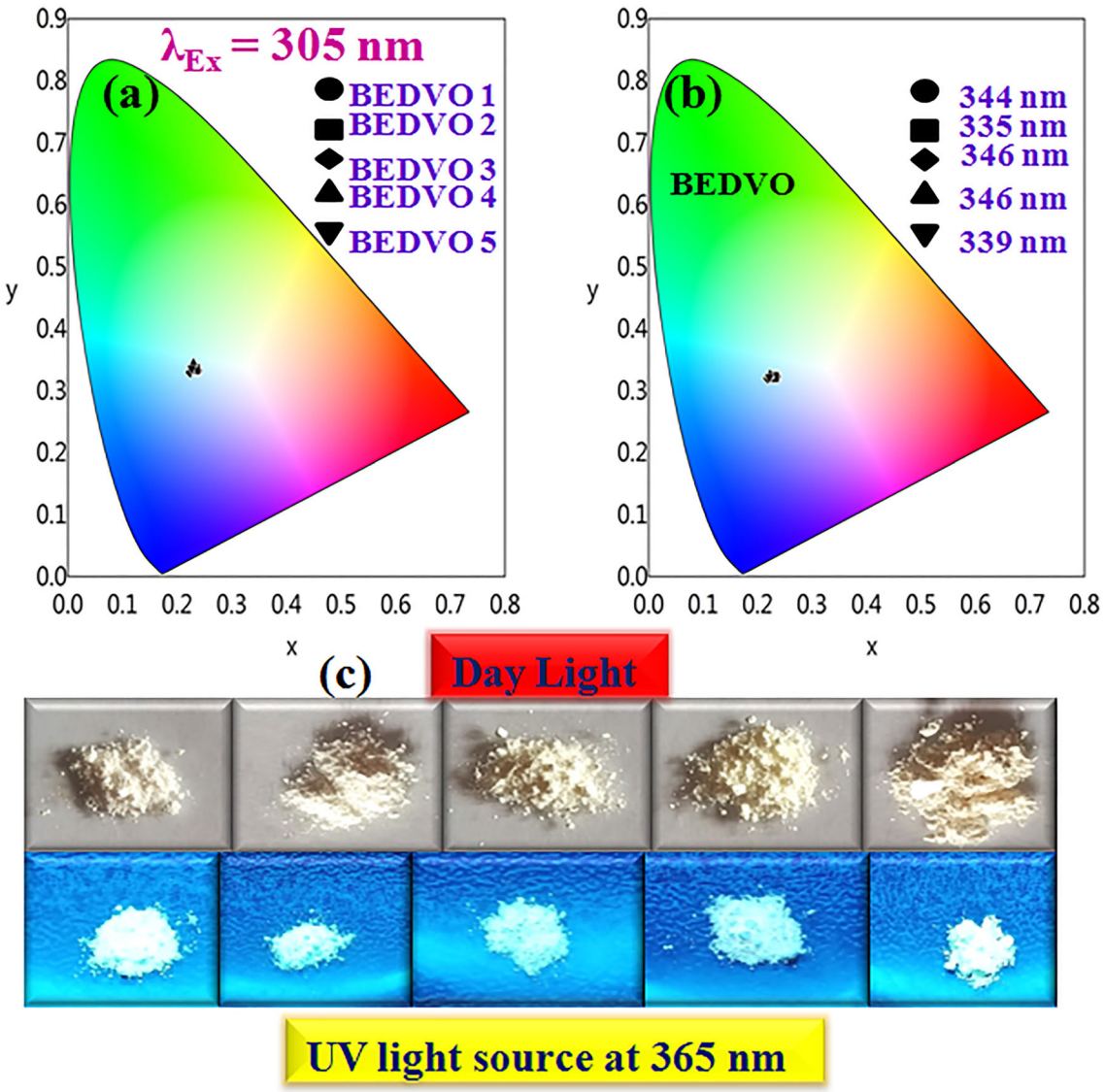

Figure 8. The CIE chromaticity diagram showing the emission colours of BEDVO phosphors excited at (**a**) 286, (**b**) 344, 335, 346, 346 and 339 nm excitations, and (**c**) images of the phosphors excited by 365 nm under a UV lamp and their corresponding daylight images.

Table 2. Comparison of CIE coordinates, CRI, CCT and their corresponding emission colours of the $Ba_{2-x}V_2O_7$:0.03Eu^{3+}, xDy^{3+} (x = 0.01, 0.02, 0.03, 0.04 and 0.05) phosphors excited at (**a**) 286 and (**b**) 344, 335, 346, 346 and 339 nm excitations.

Excitation wavelength	Dy^{3+} concentrations (x)	CIE coordinates (x, y)	RI	CCT	Emission colours
286 nm	0.01	(0.2375, 0.3320)	49	6316 K	Bluish white
	0.02	(0.2337, 0.3344)	54	6306 K	Bluish white
	0.03	(0.2239, 0.3292)	57	6268 K	Bluish white
	0.04	(0.2300, 0.3445)	53	6305 K	Bluish white
	0.05	(0.2269, 0.3371)	59	6287 K	Bluish white
344 nm	0.01	(0.2346, 0.3226)	50	6296 K	Bluish white
335 nm	0.02	(0.2310, 0.3219)	48	6283 K	Bluish white
346 nm	0.03	(0.2188, 0.3195)	44	6240 K	Bluish white
346 nm	0.04	(0.2287, 0.3200)	45	6246 K	Bluish white
339 nm	0.05	(0.2301, 0.3208)	47	6267 K	Bluish white

region and the peak broadening also decreases, which was due to the lowering of the bond distance between Eu^{3+} and O^{2-}. The luminescence property of the co-doped rare-earth ion is found to be dependent on the excitation wavelength, as a result of this finding [58].

According to Blasse's theory [59], the critical distance (R_c) of BEDVO phosphors were studied. The critical distance (R_c) is defined as the distance for which the probability of energy transfer equals to the probability of radiation emission of energy donator by the $[VO_4]^{3-}$ in the system. For BEDVO phosphor, the value of N, X_c and V were 8, 0.02 and 377.841 Å^3, respectively. The critical energy transfer distance was estimated using the Blasse's theory to 10.44 Å, which was greater than the critical distance, R_c = 5 Å. Therefore, the as-prepared BEDVO phosphors belongs to multipolar energy transfer mechanisms.

There are two types of energy transfer methods that depend on the critical distance between the sensitizer and activator ions, according to Dexter's reports [60]. They were exchanging interactions and multipolar interactions, if the value of the critical distance was about 3–4 Å. The exchange interaction may take place if the sensitizer and activator orbits overlapped. Thus, the multipolar interactions may dominate. It is concluded from the critical distance that the type of energy transfer mechanism between the sensitizer $[VO_4]^{3-}$ and the activator Eu^{3+} ion in BEDVO phosphors is thus classified as multipolar interactions. Dexture's reports reveal that the multipolar interaction takes place during the interaction between sensitizer and sensitizer or sensitizer and activator. This multipolar interaction will cause a non-radiative energy transfer. The following equation (4) determines it:

$$\frac{1}{x} = \frac{K}{1 + \beta x^{Q/3}}, \tag{4}$$

where K and β are the constants, x is the doping concentration of Dy^{3+} ions. The value of Q = 3, 6, 8 and 10, which represents the exchange interaction, dipole–dipole, dipole–quadrupole and quadrupole–quadrupole interactions, respectively [61]. Assuming $\beta x^{Q/3} \gg 1$ [62], then the above equation (4) can be simply rearranged as follows:

$$\log\left(\frac{1}{x}\right) = A - \frac{Q}{3}\log x, \tag{5}$$

where $A = \log K - \log \beta$. Figure 7 was plotted using equation (5) for $\log(1/x)$ *vs.* record (x) for Dy^{3+}-doped $Ba_2V_2O_7$ phosphor. From figure 7, the slope of the curves were obtained to be –1.45 for the emission spectra excited at 268 nm. Its corresponding Q-value was determined as 2.1025. From this result, it shows that the concentration quenching mechanism of Dy^{3+} ion in the phosphors host was due to dipole–dipole exchange interactions.

3.4 *Photometric studies*

Figure 8a and b shows the chromaticity CIE diagram of the as-synthesized BEDVO phosphors. The photographic images of the as-prepared Eu^{3+}/Dy^{3+} co-doped $Ba_2V_2O_7$ phosphors were taken in the daylight and irradiated under the UV light 365 nm. All the samples appeared to be white colour in daylight. The as-prepared BEDVO phosphors irradiated under UV light at 365 nm shows glaring white to bluish white colour, with the increase of Dy^{3+} concentration as shown in figure 8c. The CIE chromaticity coordinates, CRI and CCT values of the BEDVO phosphors were tabulated in Table 1. The CRI and CCT values were calculated from the PL emission spectra of the as-prepared BEDVO phosphors. The CCT values for the visible emission for these phosphors were calculated using McCamy's empirical [63] formula (equation (6)):

$$\mathrm{CCT} = -499n^3 + 3525n^2 - 6823n + 5520.33. \tag{6}$$

Figure 8a shows the as-synthesized phosphors excited at 286 nm, which emits bluish white colour, whereas the CCT values were slightly changed due to the doping concentration of Dy^{3+} ion. Figure 8b shows the as-prepared BEDVO phosphors excited under 344, 335, 346, 346 and 339 nm, respectively. The bluish white emission colour for all the BEDVO phosphors were observed, whereas the CCT values were changed when Dy^{3+} concentration increases. The summarized results are shown in table 2 for easy comparison. The above all, it is well demonstrated that the as-prepared BEDVO phosphors can be applicable for UV and near-UV phosphor converted WLEDs.

4. Conclusion

The hydrothermal approach was used to synthesize a series of single-phase $Ba_{1.97-x}Eu_{0.03}Dy_xV_2O_7$ (x = 0.01, 0.02, 0.03, 0.04 and 0.05). The PXRD patterns for all the BEDVO phosphors show that the dopant is substituted on the host lattice without changing the crystal system. The creation of a meta-stable state in the energy gap is confirmed by the diffused reflectance spectra, which is owing to the substitution of the Dy^{3+} ions in the as-prepared BEDVO phosphors. The PL spectra further demonstrate the doping of Dy^{3+} ion. The PL spectra obtained at 268, 344, 335, 346, 346 and 339 nm radiated a blue white colour with insignificant fluctuations in CIE coordinates. The white colour emission of BEDVO phosphors is confirmed by the irradiation under the UV light 365 nm for WLED applications. In summary, it is concluded that BEDVO phosphors have the potential ability for application in the UV and near-UV phosphor converted WLEDs.

Acknowledgement

Our deep gratitude to Dr B Sridhar, Senior Scientist, Center for X-ray Crystallography, Department of Analytical and Structural Chemistry, CSIR-Indian Institute of Chemical Technology, Ministry of Science and Technology, Government of India, Tarnaka, Hyderabad, Telangana, for his timely help in PXRD data collection.

References

[1] Fang Hongwei, Wei Xiantao, Zhou Shaoshuai, Chen Yonghu, Duan Changkui and Yin Min 2016 *Inorg. Chem.* **55** 9284
[2] Mi Xiaoyun, Kai Du, Huang Kai, Zhou Peng, Geng Dongling, Zhang Yang *et al* 2014 *Mater. Res. Bull.* **60** 72
[3] Urlagaddala Rambabu, Nagegownivari Ramachandra Munirathnam, Busireddy Sudhakar Reddy and Sandip Chatterjee 2016 *Lumin.* **31**:141
[4] Pavitra E, Seeta Rama Raju G, Jin Young Park, Lili Wang, Byung Kee Moon, Jae Su Yu *et al* 2015 *Sci. Rep.* **5** 10296
[5] Zhang Wentao, Cheng Li, Zhou Dongsheng, Zhang Li and Qiu Kehui 2018 *Ceram. Int.* **44** 5420
[6] Kewele E Foka, Birhanu F Dejene, Lehlohonolo F Koao and Hendrik C Swart 2018 *Phys. B: Cond. Matt.* **535** 245
[7] Chen Xue, Xia Zhiguo, Yi Min, Xiachan Wu and Xin Hao 2013 *J. Phys. Chem. Solids* **74** 1439
[8] Kim H, Kim J, Lim S and Park K 2016 *J. Nanosci. Nanotechnol.* **16** 1827
[9] Kumari Puja and Manam J 2016 *Chem. Phys. Lett.* **662** 56
[10] Binnemans Koen 2015 *Coord. Chem. Rev.* **295** 1
[11] Zhang Hang, Yang Hang, Li Guogang, Liu Shiqi, Li Haoran, Gong Yuming *et al* 2020 *Chem. Eng. J.* **396** 125251
[12] Ma Mingyue, Li Haidong, Cheng Fengmei and Pan Daocheng 2019 *Thin Solid Films* **676** 133
[13] Tian Li, Chen Shan-min, Liu Qiang, Jie-ling Wu, Zhao Ruini, Li Shan *et al* 2020 *Trans. Nonferrous Met. Soc. China* **30** 1031
[14] Yang Lixin, Mi Xiaoyun, Zhang Huiling, Zhang Xiyan, Bai Zhaohui and Lin Jun 2019 *J. Alloys Compd.* **787** 815
[15] Wang Yuexin, Song Yanhua, Zhou Xiuqing, Li Yi, Cui Tingting, Zheng Keyan *et al* 2016 *Chem. Eng. J.* **306** 155
[16] Chang Chengkang, Li Wen, Huang Xiaojun, Wang Zhiyu, Chen Xi, Qian Xi *et al* 2010 *J. Lumin.* **130** 347
[17] Meza-Rocha A N, Camarillo I, Lozada-Morales R and Caldiño U 2017 *J. Lumin.* **183** 341
[18] Nannan Yao, Jinzhao Huang, Ke Fu, Shiyou Liu, Dong E, Yanhao Wang *et al* 2014 *J. Power Sour.* **267** 405
[19] Sun Xin-Yuan, Han Tian-Tian, Dong-Lan Wu, Xiao Fen, Zhou Shen-Lin, Yang Qing-Mei *et al* 2018 *J. Lumin.* **204** 89
[20] Zhai Yongqing, Wang Meng, Zhao Qian, Jiabao Yu and Li Xuemin 2016 *J. Lumin.* **172** 161
[21] Vengala Rao B, Kiwan Jang, Ho Sueb Lee, Soung-SooYi and Jung-Hyun Jeong 2010 *J. Alloys Compd.* **496** 251
[22] Wang Huayu, Zhou Xuan, Yan Jinghui and Lian Hongzhou 2018 *J. Lumin.* **195** 170
[23] Chen Xin, Ding Jina, Yang Shanshan, Zhou Luhui, Chen Hongbing, Anhua Wu *et al* 2020 *J. Mod. Optic.* **67** 1078
[24] Zeng Lingwei, Tang Qiangyong, Binghua Lin Hu, Zhou Guoqing Liu, Li Youfeng *et al* 2018 *J. Lumin.* **194** 667
[25] Kaczorowska Nina, Szczeszak Agata and Lis Stefan 2018 *J. Lumin.* **200** 59
[26] Aditya Sharma, Mayora Varshney, Keun-Hwa Chae and Sung Ok Won 2018 *RSC Adv.* **8** 26423
[27] Li Fei, Fang Hongwei and Chen Yonghu 2017 *J. Rare Earth* **35** 135
[28] Santosh K G, Sudarshan V and Kadam R M 2017 *Mater. Design* **130** 208
[29] Venkatesh Bharathi N, Jeyakumaran T, Ramaswamy S and Jayabalakrishnan S S 2019 *Mater. Res. Express.* **6** 106202
[30] Simei Liu, Bin Deng, Jun Chen, Hui Liu, Chong-song Zhou and Ruijin Yu 2019 *IOP Conf. Ser.: Earth Environ. Sci.* **295** 032035
[31] Takahashi Mami, Hagiwara Manabu and Fujihara Shinobu 2016 *Inorg. Chem.* **55** 7879
[32] Rajesh Kanna R, Sakthipandi K, Senthil Kumar A, Dhineshbabu N R, Seeni Mohamed Aliar Maraikkayar S M, Afroze A S *et al* 2020 *Ceram. Inter.* **46** 13695
[33] Taniguchi Kouta, Honda Tatsuya and Kato Ariyuki 2013 *Optic. Mater.* **35** 1993
[34] Kazuki Sakoda and Masanori Hirano 2014 *Ceram. Inter.* **40** 15841
[35] Fang Mu-Huai, Meng Shu-Yi, Majewska Natalia, Lesniewski Tadeusz, Mahlik Sebastian, Grinberg Marek *et al* 2019 *Chem. Mater.* **32** 4614
[36] Liu Shiqi, Liang Yujun, Zhu Yingli, Li Haoran, Chen Jiahui, Wang Mengyuan *et al* 2018 *J. Am. Ceram. Soc.* **101** 1655
[37] Jeyakumaran T, Venkatesh Bharathi N, Sriramachandran P, Shanmugavel R and Ramaswamy S 2021 *J. Inorg. Organomet. Polym.* **31** 674
[38] Sharma A, Varshney M, Hwa Chae K and Ok Won S 2018 *RSC Adv.* **8** 26423
[39] Ri Joung M, Seong Kim J, Eun Song M and Nahm S 2009 *J. Am. Ceram. Soc.* **92** 3092
[40] Vinod Kumar, Anurag Pandey, Ntwaeaborwa O M, Viresh Dutta and Swart H C 2017 *J. Alloys Compd.* **708** 922
[41] Sajna M S, Gopi Subash, Prakashan V P, Sanu M S, Joseph Cyriac, Biju P R *et al* 2017 *Opt. Mater.* **70** 31
[42] Zhou J, Huang F, Xu J, Chena H and Wang Y 2015 *J. Mater. Chem. C* **3** 3023
[43] Cao R, Peng D, Xu H, Luo Z, Ao H, Guo S *et al* 2016 *Optik* **127** 7896
[44] Pushpendra, Kunchala R K, Achary S N and Naidu B S 2021 *ACS Appl. Nano Mater.* **2** 5527
[45] Kumari P and Manam J 2015 *RSC. Adv.* **5** 107575
[46] Pavitra E, Raju G S R, Bharat L K, Park J Y, Kwak C H, Chung J W *et al* 2018 *J. Mater. Chem. C* **6** 12746
[47] Niu P, Liu X, Wang Y and Zhao W 2018 *J. Mater Sci: Mater. Electron.* **29** 124
[48] Tang Q, Qiu K, Li J, Zhang W and Zeng Y 2017 *J. Mater. Sci. Mater. Electron.* **28** 18686
[49] Astha Kumari, Vineet Kumar Rai and Kaushal Kumar 2014 *Spectrochim. Acta Part A* **127** 98
[50] Sasank Pattnaik and Vineet Kumar Rai 2020 *J. Mater. Res. Bull.* **125** 110761
[51] Dhobale A R, Mohapatra M, Natarajan V and Godbole S V 2012 *J. Lumin.* **132** 293
[52] Kai Li and Rik Van Deun 2019 *ACS Sustain. Chem. Eng.* **7** 16284

[53] Pushpendra, Sarabjot Singh, Saumya Srinidhi, Kunchala Rimple Kalia *et al* 2021 *Cryst. Growth Des.* **21** 4619
[54] Pushpendra, Indranil Suryawanshi, Saumya Srinidhi, Sarabjot Singh, Rimple Kalia, Kunchala R K *et al* 2021 *Mater. Today Commun.* **26** 102144
[55] Pushpendra, Indranil Suryawanshi, Rimple Kalia, Kunchala R K, Shyam Lal Mudavath and Naidu B S 2022 *J. Rare Earths* **40** 572
[56] Kai Li and Rik Van Deun 2020 *ACS Appl. Electron. Mater.* **2** 1735
[57] Pushpendra, Kunchala R K, Achary S N, Tyagi A K and Naidu B S 2019 *Cryst. Growth Des.* **19** 3379
[58] Zhou Jiangcong, Feng Huang JuXu, Chen Hui and Wang Yuansheng 2015 *J. Mater. Chem. C* **3** 3023
[59] Liu Jun, Deng Huawei, Zhang Yueli, Chen Dihu and Shao Yuanzhi 2015 *Phys. Chem. Chem. Phys.* **17** 15412
[60] Wu X, Bai W, Hai O, Ren Q, Lin F and Jiao Y 2018 *J. Solid State Chem.* **265** 109
[61] Shinde K N, Singh R and Dhoble S J 2014 *J. Lumin.* **145** 588
[62] Hao Chiang C, Yu Lin H and Yuan Chu S 2014 *J. Am. Ceram. Soc.* **97** 3737
[63] Zhang W, Shen H, Hu X, Wang Y, Li J, Zhu Z *et al* 2019 *J. Alloys Compd.* **781** 255